J Mater Sci: Mater Electron (2016) 27:1847–1853
DOI 10.1007/s10854-015-3963-6

Effect of Fe doping on structural, optical and photocatalytic activity of WO_3 nanostructured thin films

S. Ramkumar[1] · G. Rajarajan[2]

Received: 7 September 2015 / Accepted: 23 October 2015 / Published online: 30 October 2015
© Springer Science+Business Media New York 2015

Abstract We have successfully synthesized pure and iron (Fe) doped tungsten trioxide (WO_3) and nanothin films were deposited by chemical bath deposition method on glass substrates coated with FTO (F-doped tin oxide). The as-deposited films were annealed at 600 °C for 2 h in ambient atmosphere in order to improve crystallinity and structural perfection. The effect of Fe doping on structural, optical, and morphology of thin films was analyzed by X-ray diffraction (XRD), Fourier transform infra-red (FTIR) spectra, UV–Vis spectra, Photoluminescence (PL), and Atomic force micrograph (AFM) images. The XRD measurements showed that both the pristine and Fe doped WO_3 films crystallize in monoclinic structure and the results are in good agreement with the standard JCPDS data (Card no: 83-0950). The surface of the films are very smooth and the calculated roughness value is around 28–17 nm, which is in good agreement with the average crystallite sizes calculated by Scherrer's formula. The optical band gap energy of was found to be decreased from 3.12 to 2.92 eV with increase of Fe concentrations (0–10 wt%). The photocatalytic activities of the films were evaluated by degradation of methylene orange (MO and Phenol in an aqueous solution under visible light irradiation. The photocatalytic activity of Fe (10 wt%) doped WO_3 film was much higher than that of the pure WO_3. The improved photocatalytic mechanism by Fe doping is also discussed.

✉ S. Ramkumar
ramkumarphd2015@gmail.com

[1] Department of Physics, Oxford Engineering College, Tiruchirappalli, Tamilnadu 620 009, India

[2] Department of Physics, Vidhya Mandhir Institute of Technology, Erode, Tamilnadu 638 052, India

1 Introduction

Waste water from textile, paper and some other industries include residual dyes, which are not gladly biodegradable. Heterogeneous photocatalysis has been proved to be a capable technique for the elimination of these pollutants from aqueous and gaseous media [1]. Nanostructure metal oxide thin films have concerned considerable interest because of their potential applications such as gas sensor, solar cell, bio sensor, and photocatalyst [2]. Recently various semiconducting metal oxide, such as TiO_2, SnO_2, ZnO, WO_3, CdO, were investigated as photocatalytic materials. Among them, tungsten trioxide (WO_3) is one of the most interesting materials exhibiting a wide variety of novel properties particularly in thin film form. WO_3 is an n-type semiconductor, has numerous interesting physical and chemical properties suggesting the potential use of this material in a multitude of applications such as photocatalysis, gas sensors, batteries, photoluminescence, electrochromic, and photo oxidation of water [3]. Many synthesis methods have been adapted to deposit the WO_3 thin films such as, thermal evaporation [4], electron beam evaporation [5], chemical vapour deposition [6], and laser deposition [7] methods. Compared with the above methods, the chemical bath deposition method (CBD) is one of the suitable methods for preparing highly efficient thin films in a simple manner. The growth of thin films strongly depends on growth conditions, such as duration of deposition, composition and temperature of the solution, and topographical and chemical nature of the substrate. Chemical bath deposition yields stable, adherent, uniform and hard films with good reproducibility by a relatively simple process [8]. A sufficient degree of crystallinity is required to attain the desired electronic properties necessary for photocatalytic applications. This can be achieved through

annealing the films (catalyst) materials at higher temperatures (600 °C/2 h) and atmospheres. On the other hand, tuning the band gap and morphology of photocatalytic materials is the important way to enhance the photocatalytic efficiency of photocatalytic materials [9]. Many metal elements such as Mg, Zn, Fe, Mo, V and Ti have been applied to tune the band gap and improve the photocatalytic performance of WO_3 [10]. Especially, due to the enhancement of the absorption of visible light and effective separation and transformation of the photo-excited electrons and holes. Fe element has gained more and more attention in narrowing the band gap of WO_3. Moreover Fe element can easily substitute in the WO_3 host lattice due to the similar size of WO_3, these results can expect to increase the photocatalytic performance.

So, in the present work, we have choosing Iron (Fe^{3+}) metal ions dopant, in order to improve the photocatalytic efficiency and the role of Fe dopants on structural, optical and photocatalytic activity of WO_3 films. To the best of our knowledge, this is the first preliminary report about structural, optical and photocatalytic activity of Fe doped WO_3 films by chemical bath deposition method.

2 Experimental procedure

2.1 Preparation of Fe–WO_3 thin films

Tungstic acid (H_2WO_4) and Iron nitrate nonahydrate ($Fe(NO_3)_3{\cdot}9H_2O$) were used as tungsten and iron sources, respectively. The starting solution was prepared by mixing of tungstic acid in 10 ml of sodium hydroxide (NaOH) solution. It resulted in a yellow color solution due to proton exchange protocol process. Appropriate amount of Fe $(NO_3)_3{\cdot}9H_2O$ in (0, 5 and 10 wt%) deionised water was added to the above solution. pH of the sol was adjusted to 2 with the addition of 2 ml of HCL. The dropping rate must be well controlled for the chemical homogeneity. Films were grown on 76 mm × 26 mm × 1 mm glass microscope slides which were used as depositing substrates. The glass slides as the substrates for depositing Fe–WO_3 films were prepared by ultrasonically cleaned by acetone, followed by ethanol and finally, deionized water for 10 min respectively and allowed to air dry. The substrate was suspended vertically in the reaction bath after stirring the solution properly for homogeneity. The thin film samples were deposited at the temperature between 60 and 70 °C for 1 h. The as-deposited thin films were annealed at 600 °C for 2 h in muffle furnace, in order to improve the crystanility. Pure WO_3 thin films were prepared in a similar manner without the use of iron source. The schematic representation of chemical bath deposition method is shown in Fig. 1.

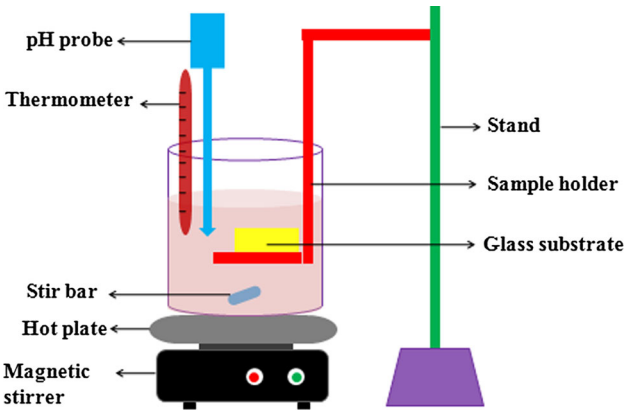

Fig. 1 Schematic representation of chemical bath deposition method

2.2 Characterization techniques

The prepared samples (annealed) were successfully characterized by the following techniques. Structural properties of the Fe–WO_3 thin films were analyzed by using X-ray diffraction (XRD, JEOL diffractometer) with monochromatized Cu Kα radiation (λ = 1.54056 Å) in the range of 10°–80° with the step size of 0.1°. Fourier transform infrared measurements were recorded by using Technos instruments (Seki technotron Corp, Japan) in the range of 200–1000 cm^{-1}. The optical transmittance of the thin films was recorded at room temperature by a Perkin Elmer UV/VIS/NIR Lambda 19 spectrophotometer in the wavelength range of 300–900 nm. The morphology of the Fe–WO_3 thin films is observed by Atomic force microscope (ParkXE100 AFM non-contact mode). Photoluminescence spectra of the samples were recorded using PerkinElmer LS 55 Spectrometer equipped with a 40 W Xenon lamp, Excitation length used was 325 nm.

3 Results and discussion

3.1 XRD analysis

Non-destructive X ray diffraction technique was used to determine the phase purity, crystallinity and structural analysis of the pure and Fe doped WO_3 thin films as shown in Fig. 2. It was noted that both the pure and Fe doped WO_3 films had a monoclinic type crystal structure and the following miller indices and the results are good in agreement with the standard JCPDS data values (card no: 83–0950). There are no secondary phases (WO_3 H_2O, Fe_2O_3 and Fe) were observed except WO_3, this result indicate the good crystanality of the films. It was also noted that the broadening and the peak intensity was decreases with the increase of Fe content. The lattice parameters of

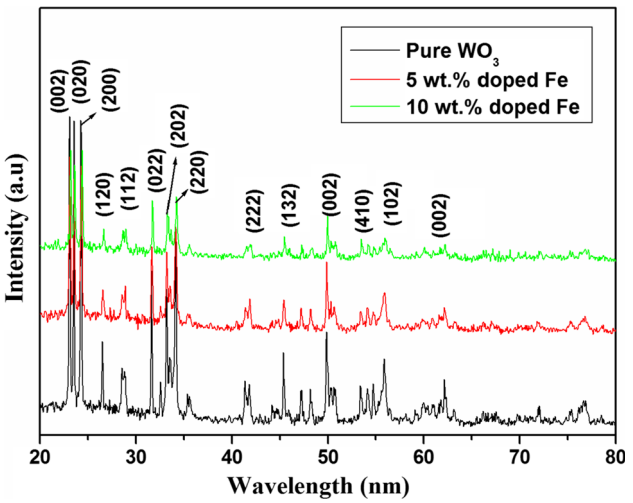

Fig. 2 Powder XRD pattern of WO_3 thin film with different Fe content

pure WO_3 were estimated at a = 7.3692 (Å), b = 7.5376 (Å) and c = 7.6231 (Å). After Fe doping, these parameters decrease with the increase in the zinc concentrations (Table 1), the observed variation in lattice parameters was consistent with the smaller radius of the Fe^{3+} ion (0.76 Å) with respect to the W^{6+} ion radius (0.78 Å) and with the small amount of iron concentration used for doping.

The average crystalline sizes of the pure and Fe doped WO_3 nanothin films were calculated by using Scherrer's equation [11].

$$d = \frac{K\lambda}{\beta \cos\theta}$$

where d is the mean crystallite size, K is the shape factor taken as 0.89, λ is the wavelength of the incident beam, β is the full width at half maximum and θ is the Bragg angle. The average crystalline size of pristine WO_3 was found to be 28 nm and it was further decreased to 17 nm for 10 wt% Fe doped WO_3. These results clearly indicate that Fe^{3+} substituted in WO_3 host lattice site.

3.2 Atomic force microscope analysis

Atomic force microscopy (AFM) is a useful technique to determine the surface morphology and particle size of the samples. Figure 3 shows the 2D and 3D AFM image of pure and Fe doped WO_3 thin films. It was clear evidence that the particle distribution is uniform and particle size reduces with increase in Fe amount in these films. For an optical surface, roughness is normally considered as an important parameter. Surface roughness is not only the light scattering but also give an idea about the quality of the surface under investigation, in addition to providing some insight on the growth morphology. A systematic description of various analytical method used for roughness characterization can be found in Ref. [12]. Root mean square roughness (R_{rms}) which is defined as standard deviation of the surface height profile from the mean height, is the most commonly reported measurement of the surface roughness and is given by,

$$R_{\text{rms}} = \left[\frac{1}{N}\sum_{i}^{n}(h_i - \langle h\rangle)^2\right]$$

where N is the number of pixels in the image h_i is the height of ith pixel and <h> is the mean height. The R_{rms} values of pristine and Fe (5 and 10 wt%) doped WO_3 were found to be 29, 23, 19 nm respectively. These values are good in agreement with the crystalline size calculated from XRD results.

3.3 UV–Vis transmission spectra analysis

In order to confirm the optical property and substitution of Fe into WO_3 site, the films were characterized by UV–Vis transmission spectra analysis. Figure 4a shows the UV–Vis transmission spectra analysis of pure and Fe doped WO_3 films. Both the films are highly transparent in the visible region and a sharp fall in transmission is observed below 400 nm region. In Fe doped films, the absorption band decreases and shifts toward longer wavelength (red shift) with doping of Fe ion. In order to determine the optical band gap of the films, we assume that the direct transition takes place in these films, and the absorption coefficient was fitted to the Tauc's relation:

The absorption coefficient (α) was calculated from the transmission spectra using equation [13],

$$\alpha = 1/t \ln(1/T)$$

where T is the optical transmission and t is the film thickness. The direct band gap of thin films was calculated from Fig. 4b using the formula [14],

Table 1 Shows the lattice parameters and average crystallite size of WO_3 nanothin films with different Fe concentrations

Fe concentrations (wt%)	Crystallite size (nm)	Lattice parameter values		
		a (Å)	b (Å)	c (Å)
0	28	7.3692	7.5376	7.6231
5	23	7.3659	7.5356	7.6221
10	17	7.3601	7.5321	7.6199

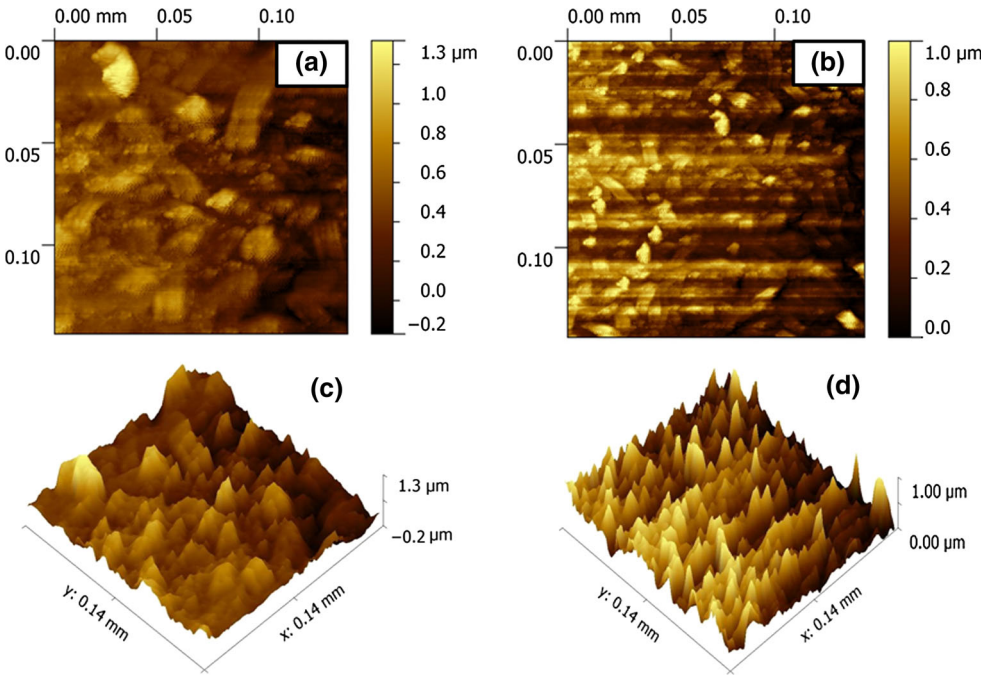

Fig. 3 AFM micrograph (2D image) of WO_3 thin film with different Fe content **a** pure WO_3, **b** Fe 10 wt%: 3D image of WO_3 thin films, **c** pure WO_3, **d** Fe 10 wt%

$$\alpha hv = A(hv - E_g)^m$$

where α is the absorption coefficient, h is the Planck's constant, ν is the frequency of incident light, E_g is the energy band gap of material and m is the factor governing the direct/indirect, etc. transition of electron from the valance band to the conduction band. The band gap energy was calculated as 3.12, 3.04 and 2.92 eV for pure and Fe (5 and 10 wt%) doped WO_3 films (Fig. 4b). The decrease in the band gap for Fe-doped WO_3 films is due to the doping of iron which creates impurity levels below the conduction band of WO_3. Similar findings were observed in Fe doped WO_3 thin films by spin coating method [15].

3.4 Photoluminescence spectra analysis

PL emission spectrum has been widely used to investigate the efficiency of charge carrier trapping, migration and transfer, and to understand the fate of electron hole pairs in the semiconducting oxide materials [16]. Figure 5 shows the PL emission spectra of both pure and Fe doped WO_3 films measured from 300 to 600 nm using a 325 nm He–Cd laser. In both the films, series of peaks were observed at 360, 412 and 436, 490 and 520 nm. The UV emission (360 nm, 3.5 eV) corresponds to the structural defects and decreases the band gap energy. The decreasing in band gap energy was already confirmed in UV–Vis spectra analysis. The emissions bands at 412, 436 and 487 nm were defect-related to electron transition mediated by defect levels in the band gap, such as oxygen vacancies [16]. The green emission peak (520 nm) is related to V_o^+ oxygen vacancies, this emission may be attributed to the different luminescent centers such as defect energy levels arising due to tungsten interstitials and oxygen vacancies as well as dangling bonds into nanocrystals. The intensity of all the peaks decreases with the increase of the Fe content. Moreover the shifting of peak may be due to the presence of Fe dopant in WO_3 and can cause lattice defects.

3.5 FTIR spectra analysis

Fourier transform infrared (FTIR) spectroscopy is a useful technique that provides information about the chemical bonding or molecular structure of materials [17]. Figure 6 shows FTIR spectra of pure and Fe doped WO_3 (5 and 10 wt%) samples in room temperature. The absorption bands at 3423.12 cm^{-1} attributed to stretching vibration of surface hydroxyl group or adsorbed water, which is probably due to the fact that re-adsorption of water from the ambient atmosphere has occurred [18]. The vibration bands at 1592.34 and 1486.23 cm^{-1} are related to the vibration of tungsten-hydroxyl (W–OH) bond. The spectrum shows strong band at 800–600 cm^{-1} range for W–O–W bridging mode [18]. A weak band at ~626.12 cm^{-1} is associated with the O–W–O when hydrogen was located at a coplanar square of oxygen atoms. So the FTIR results again confirmed the presence of WO_3 phase with crystalline nature.

3.6 Photocatalytic activity set up

The photocatalytic activity setup was fabricated by Vadivel et al. [19]. The detailed experimental set up was described

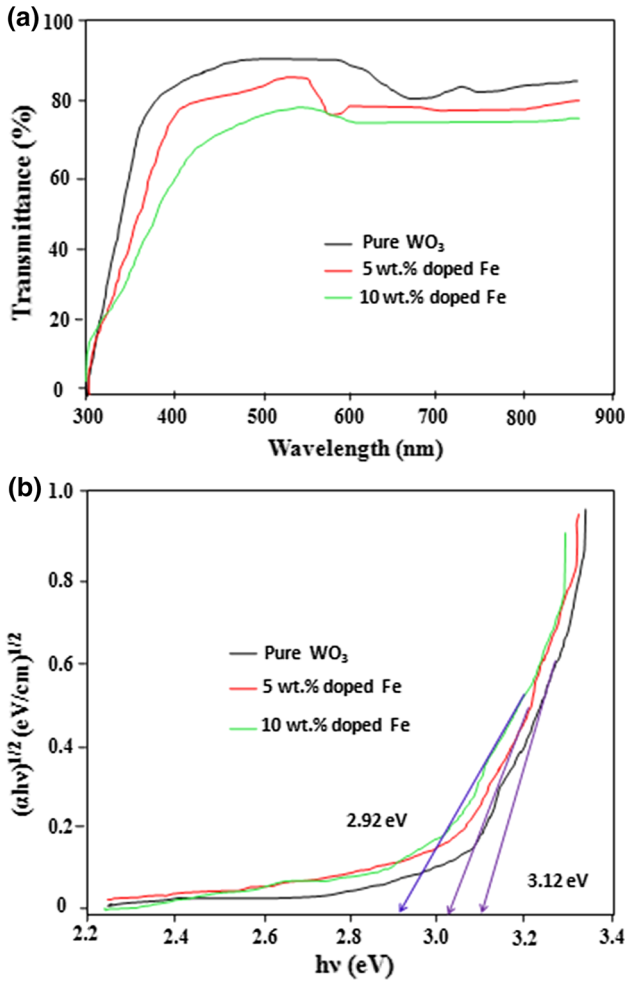

Fig. 4 UV–Vis spectra of WO_3 thin film with different Fe content **a** transmittance spectra, **b** band gap energy determination

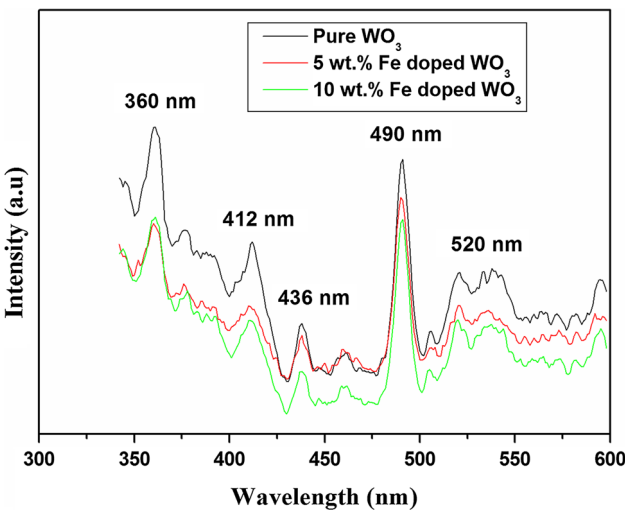

Fig. 5 Photoluminescence spectra of pure and Fe doped WO_3 thin films

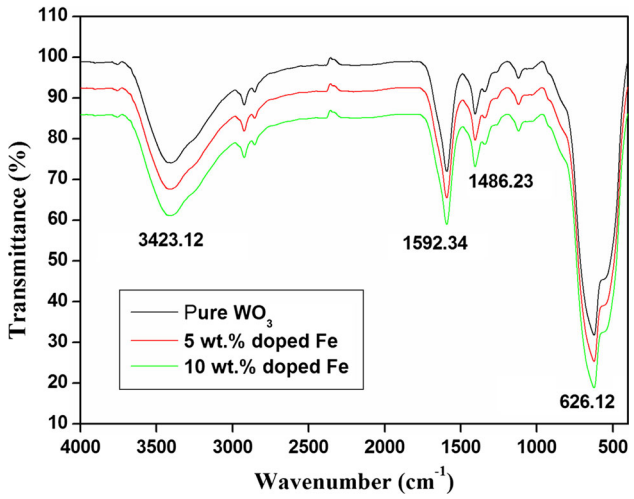

Fig. 6 FTIR spectra of WO_3 thin film with different Fe content

below. Photocatalytic experiment on the prepared samples for the photodegradation of dyes is performed at ambient temperature. The photocatalytic activities of Fe doped WO_3 films were evaluated by the degradation of two types of dyes, including methylene orange (MO) and Phenol solution, in visible light irradiation. For photocatalytic process, two pieces of 25 mm × 75 mm glass plate coated with films were settled into 25 ml of dye solutions (MO and Phenol) with a concentration of 15 mg/l in a 100 ml cylindrical glass reactor. The 125 W high pressure mercury lamp was used as a light source. The coated glass/dye solution was irradiated in the horizontal direction and the distance between the UV lamp and the glass/dye solution was kept within 25 cm. Then the solution has to be kept in the dark room and well stirred with the magnetic stirrer for more than 30 min to attain the equilibrium condition throughout the solution. The concentration of the aqueous suspensions (MO and Phenol) in each sample was analyzed using UV–Vis spectrophotometer at a wave-length of 664 nm. The photocatalytic efficiency has been calculated from the expression $\eta = (1 - C/C_0)$, where C_0 is the concentration of dyes (MO and Phenol) before illumination and C is the concentration of dyes after a certain irradiation time.

3.6.1 Photocatalytic activity measurements

The photocatalytic activities of pure and Fe doped WO_3 samples were evaluated based on their ability to degradation of various dyes such as, methyl orange (MO) and Phenol under visible irradiation. The results showed that the time of the illumination and the quantity of the photocatalyst have obvious influence on the degradation of the reactive dyes. Figures 7 and 8 present the degradation

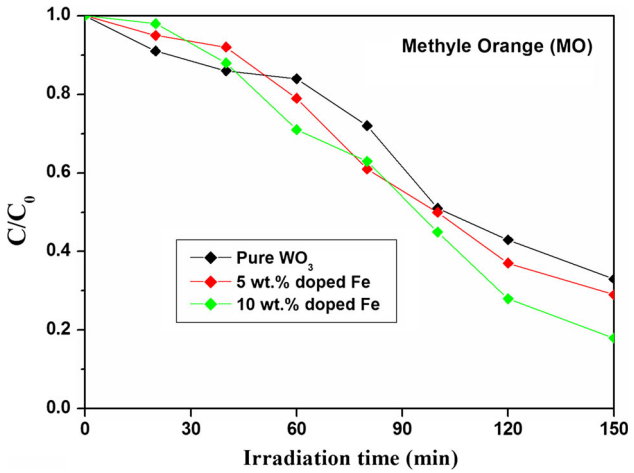

Fig. 7 Photocatalytic degradation of methyle orange (MO) using Fe–WO_3 thin films under visible-light irradiation

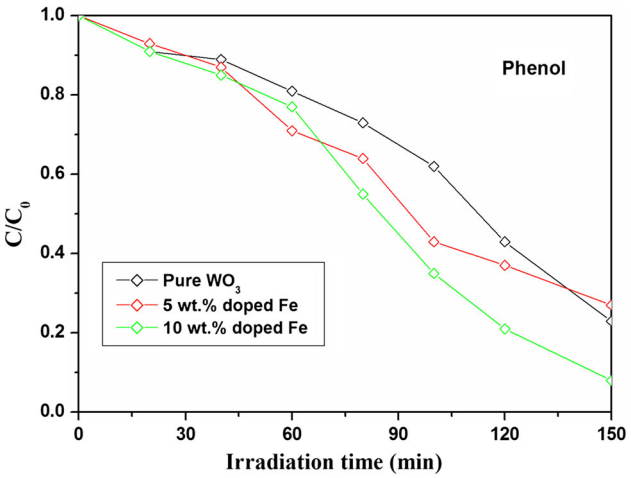

Fig. 8 Photocatalytic degradation of phenol using Fe–WO_3 thin films under visible-light irradiation

profiles of MO and Phenol the presence of WO_3 with different Fe concentrations (5 and 10 wt%). In Figs. 7 and 8, we have plotted the graph between degradation percentage of MO & Phenol dyes concentration in the aqueous sample after visible light illumination in the presence of a typical pure and Fe doped WO_3 samples. The decrease of MO and phenol concentration in the presence of pure WO_3 was very small. However, the photocatalytic activities had been improved when WO_3 was doped by Fe. With the reaction time at 150 min, the MO degradation efficiencies of pure and Fe (5 and 10 wt%) doped WO_3 samples are about 67, 71, and 82 %, respectively. Similarly the Phenol degradation efficiencies of pure and Fe (5 and 10 wt%) doped WO_3 samples are about 73, 79 and 92 %, respectively. The above results, we concluded that the photocatalytic performances of the Fe-doped WO_3 have outstanding enhancements compared to the pure WO_3 under visible-light illumination. The reusability of the Fe (10 wt%) doped WO_3 samples as photocatalyst is also studied by collecting and reusing the same photocatalyst for multiple cycles. As shown in Fig. 9, after 7 runs of photodegradation of Phenol, the photocatalytic activity of the Fe–WO_3 samples shows a slight degeneration due to incomplete recollection and loss during washing. Thus, the Fe–WO_3 samples used as photocatalyst are quite stable and have enormous potential application in water treatment. The phocatalytic mechanism of Fe–WO_3 catalyst is shown in Fig. 10.

The doping Fe^{3+} ions can create a donor level above the valence band of WO_3 to increase the absorption intensity of visible light [20]. The donor level was much more distant from the valence band with the increasing of iron content. Consequently, huge numbers of electrons could be excited under visible light region, which could also efficiently enhance the photocatalytic performance. In addition, Fe dopant could decrease the band gap energy of the pristine

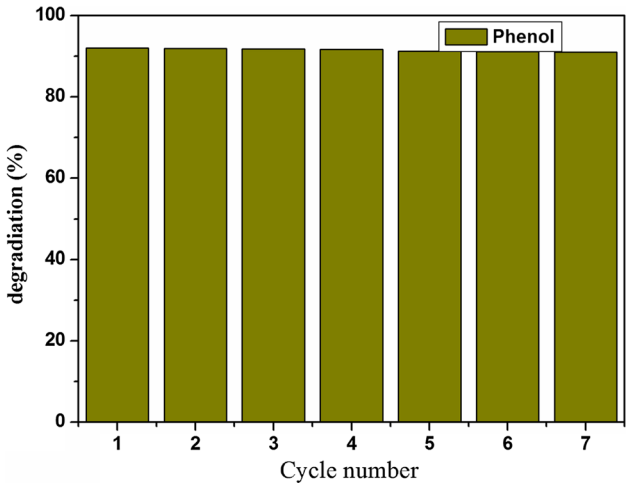

Fig. 9 7 cycles of degradation of Phenol using Fe–WO_3 thin films as the photocatalyst

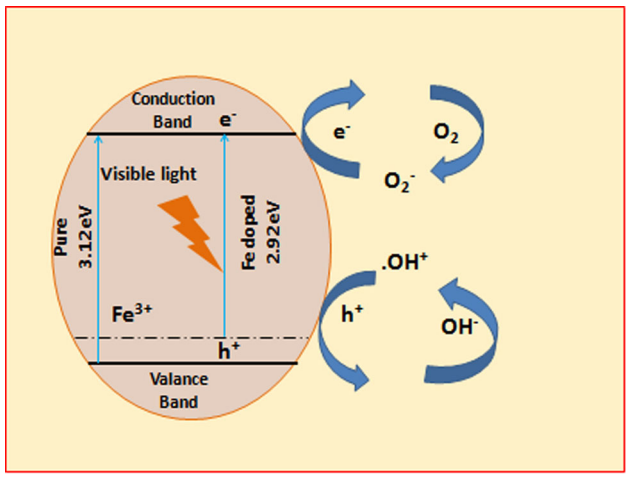

Fig. 10 Schematic representation for photocatalytic mechanism of Fe doped WO_3 catalyst

WO_3. Fe^{3+} ions could trap and transfer electrons and holes to inhibit the recombination of photo-excited holes and electrons [21], and the smaller band gap energy due to Fe dopant may play another role in enhancing the visible light photocatalytic activity of WO_3 films.

4 Conclusions

In summary, we have successfully synthesized pristine and Fe doped WO_3 nanostructured thin films by simple chemical bath deposition method. XRD and AFM results suggest that grain growth is suppressed due to Fe doping and the calculated crystalline size and surface roughness value is well matched. The optical band gap energy of the Fe-doped WO_3 could be tuned by controlling Fe doping contents. The defect in samples such as oxygen vacancies and decreasing the band gap energy play a crucial role, which is confirmed by photoluminescence spectra analysis. The Fe (10 wt%) doped WO_3 films had the highest photocatalytic efficiency under visible light irradiation with presence of MO and Phenol dyes. This is due to separation charge carries between electron–hole pairs. This Fe doped WO_3 catalyst may have potential applications in pollutant removal as a highly efficient photocatalyst.

References

1. J.M. Herrmann, Catal. Today **53**, 115–129 (1999)
2. A. Herzing, C.J. Kiely, A.F. Carley, P. Landon, G. Hutchings, J. Sci. **321**, 1331 (2008)
3. V. Hariharan, S. Radhakrishnan, M. Parthibavarman, R. Dhilipkumar, C. Sekar, Talanta **85**, 2166–2174 (2011)
4. A. Antonaia, T. Polichetti, M.L. Addonizio, S. Aprea, C. Minarini, A. Rubino, Thin Solid Films **354**, 73–81 (1999)
5. A.A. Joraid, S.N. Almari, Phys. B Phys. Condens. Matter **391**, 199–205 (2007)
6. P. Tagtstrom, U. Jansson, Thin Solid Films **352**, 107–113 (1999)
7. O.M. Hussain, A.S. Swapnasmitha, J. John, R. Pinto, Appl. Phys. A **81**, 1291–1297 (2005)
8. S. Vadivel, G. Rajarajan, J. Mater. Sci. Mater. Elect. **26**, 3155–3162 (2015)
9. X.W. Lou, L.A. Archer, Z. Yang, Adv. Mater. **20**, 3987–4019 (2008)
10. C. Feng, S. Wang, B. Geng, Nanoscale **3**, 3695–3699 (2011)
11. M. Parthibavarman, B. Renganathan, D. Sastikumar, Curr. Appl. Phys. **13**, 1537–1544 (2013)
12. J.M. Bennett, L. Mattson, *Introduction to Surface Roughness and Scattering* (Optical Society of America, Washington, 1989)
13. S.S. Roy, J. Podder Gilberto, J. Optoelect. Adv. Mater. **12**, 1479–1484 (2010)
14. R.K. Nath, S.S. Nath, K. Sunar, J.Anal. Sci. Technol. **3**, 85–94 (2012)
15. R. Dhunna, P. Koshy, C.C. Sorrell, J. Aust. Ceram. Soc. **51**, 18–22 (2015)
16. P. Wu, Q. Li, X. Zou, W. Cheng, D. Zhang, C. Zhao, L. Chi, T. Xiao, J. Phys. Conf. Ser. **188**, 012054 (2009)
17. S.M. Ali, J. Muhammad, S.T. Hussain, S.A. Bakar, M. Ashraf, K. Naeem-ur-Rehman, J. Mater. Sci. Mater. Electron. **24**, 2432–2437 (2013)
18. U. Opara Krasovec, A. Surca Vuk, B. Orel, Electrochim. Acta **46**, 1921–1929 (2001)
19. S. Vadivel, G. Rajarajan, J. Mater. Sci. Mater. Elect. **26**, 5863–5870 (2015)
20. R. Dholam, N. Patel, M. Adami, A. Miotello, Int. J. Hydrog. Energy **34**, 5337–5346 (2009)
21. H. Song, Y. Li, Z. Lou, M. Xiao, Z. Ye, L. Zhu, Appl. Catal. B **166–167**, 112–120 (2015)